Parallel optical arithmetic on images by a redundant binary number representation

Giuseppe A. De Biase and Annalisa Massini

La Sapienza University of Rome, Astronomy Institute, 29 Via G. M. Lancisi, I-00161 Rome, Italy.

Received 12 June 1989.
0003-6935/90/111587-03$02.00/0.

A redundant binary number representation allows the algebraic sum on signed numbers in constant time. This number representation is suitable for parallel arithmetic on images made by symbolic substitution on optical computers. Key words: Optical computing, image arithmetic, redundant number representation.

Quick and efficient processing of images is an important request of various disciplines and several applied fields. Many authors have studied specialized computing architectures (with electronic technology) devoted to image processing (see, for example, Refs. 1–5), but other authors have pointed out that optical computing architectures are more suitable for massive computation on images because of the 2-D inherent structure both of data (images) and DOC (digital optical computing) architectures.

In recent works[6,7] Huang *et al.* showed a complete formal approach to a 2-D binary algebra and related arithmetic oriented to 2-D objects. In the second work (regarding a parallel optical arithmetic on images, with emphasis on the symbolic substitution method[8–11]) the use of redundant number representations is neglected in spite of several works about this subject related to optical computing systems. Redundant number systems can have important properties such as the carry-free addition (namely, the possibility to carry out addition in constant time independent of the bit strings length k).[12–16]

In optical image arithmetic a novel redundant binary (RB) number representation[17] can be used. In the RB representation an integer D is given by

$$D = \sum_{i=0}^{k-1} a_i 2^{i-[i/2]} \qquad \text{with } k \text{ even},$$

where $a_i \in \{0,1\}$, i is the position index, and k is the length of the bits string. Each RB number has a canonical form and several redundant representations. If, following the work of Huang *et al.*,[7] the bits are symbol coded as

$$0 \rightarrow \square \quad \text{and} \quad 1 \rightarrow \blacksquare,$$

the RB numbers canonical form can be obtained—from the symbol coded natural binary representation—by the following simple rules:

$$\square \rightarrow \square\,\square \quad \text{and} \quad \blacksquare \rightarrow \square\,\blacksquare$$

(the formal definition of the RB and p-RB redundant number representations, their properties, and efficiencies will be presented in Ref. 17).

Using RB numbers, a constant time addition [instead of $O(k)$ time of Ref. 7] can be performed by symbolic substitution, by applying the rules introduced in Fig. 1 twice on the operands (see also Fig. 2).

The RB representation has several advantages if compared with other redundant number representations, as, for example, the modified signed digit (MSD) one (widely studied for optical computing).[13–15] RB representation is particularly suitable for machines with a two-valued logic, it allows the parallel encoding of signed numbers in 2s complement (in simply one step), and consequently, it allows use of the addition algorithm as the algebraic sum on signed numbers. This avoids the necessity of separate rules for the subtraction, and one table only is needed for the whole arithmetic. Finally, the multiplication can be obtained in $O(\log_2 k)$ time.[18]

The decoding of an RB number can be performed simply

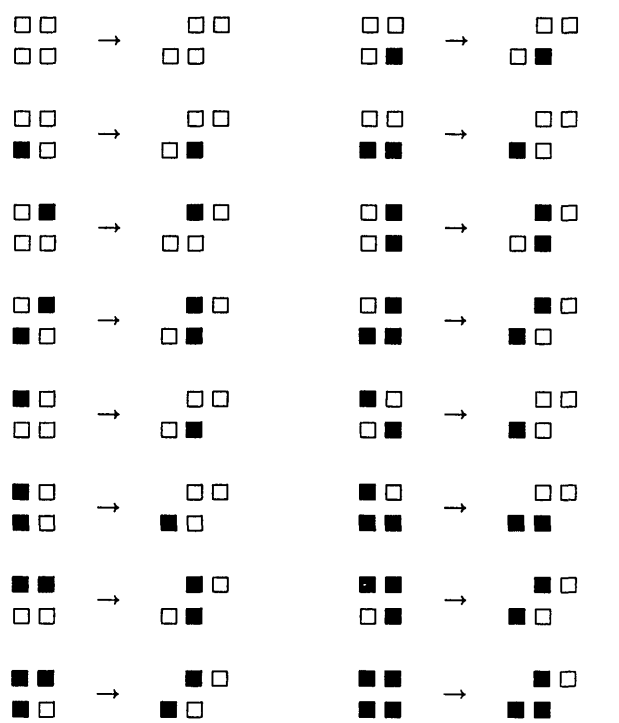

Fig. 1. Symbolic substitution rules for the addition of unsigned RB numbers or for the algebraic sum of signed ones. These rules act on symbol pairs on two rows (see Fig. 2), the output lower pair is shifted left one position.

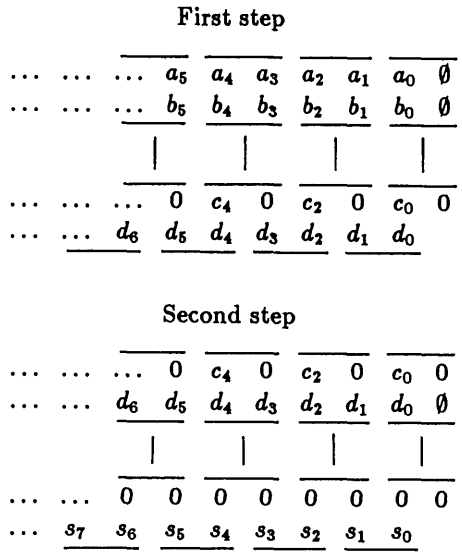

Fig. 2. Parallel application of addition symbolic substitution rules on two strings of symbols. At each step the input and the output are on two strings: a_i and b_i are the bits of the inputs operands, c_i and d_i are the bits of the intermediate sums, and s_i are the bits of the result. The symbol $\emptyset$ is a padded zero. At the last step the upper string is zeroed.

by one shift and one binary addition, in fact the decoded value B—in natural binary representation—is given by

$$B = B_{\text{even}} + 2B_{\text{odd}},$$

where

$$B_{\text{even}} = \sum_{i=0}^{k-2} a_{i_{\text{even}}} 2^{i_{\text{even}}}$$

and

$$B_{\text{odd}} = \sum_{i=1}^{k-1} a_{i_{\text{odd}}} 2^{i_{\text{odd}}},$$

with k even. The nonconstant time complexity in the decoding operation is not particularly important because this operation is used only when the data must be given to the external world.

A property of the RB numbers addition, performed with the rules of Fig. 1, is that the addition of two strings considered as the concatenations of many RB numbers gives a resulting string which is the concatenation of RB sums (if the numbers on each string are separated by at least a pair □ □ in the same positions on the two operands).[17] This property guarantees that the addition of all pixel pairs on a row coded image (see Fig. 3, and Ref. 7) or the addition of two row coded images can always be performed in parallel in two steps, independent of the number of bits per pixel used (and of the image dimension).

An RB numbers arithmetic can easily be implemented on both optical and electronic systems making easier the attainment of hybrid machines particularly suitable for image processing.[19,20]

This work was carried out within the framework of Progetto Finalizzato Sistemi Informatici e Calcolo Parallelo of CNR (National Research Council).

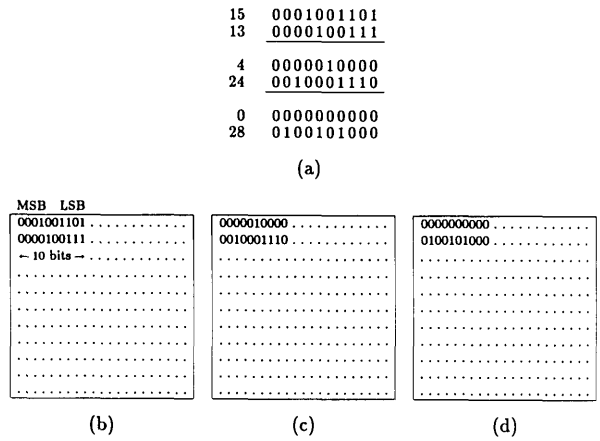

Fig. 3. Parallel addition on a row coded image (the pixels are 10 bits wide and in RB representation): (a) example of the addition, (b) operands on a row coded image, (c) first step (image with intermediate sums), (d) second step (image with results).

References

1. M. J. B. Duff and S. Levialdi, Eds., *Languages and Architectures for Image Processing*, (Academic, London, 1981).
2. H. Matzushima, T. Uno, and M. Ejiri, "An Array Processor for image processing," in *Real-Time Parallel Computing*, M. Onoe, K. Preston, and A. Rosenfeld Eds. (Plenum, New York, 1981), p. 325.
3. P. E. Danielsson and S. Levialdi, "Computer Architectures for Pictorial Information Processing," Computer, Nov., 53–67, (1981).
4. A. P. Reeves, "Parallel Computer Architectures for Image Processing," Comput. Vision Graphics, Image Process. **25,** 68–88 (1984).
5. E. W. Kent, M. O. Shneier, and R. Lumia, "PIPE (Pipelined Image-Processing Engine)," J. Parallel Distributed Comput. **2,** 50–78 (1985).
6. K.-S. Huang, B. K. Jenkins, and A. A. Sawchuk, "Binary Image Algebra and Optical Cellular Logic Processor Design," Computer Vision, Graphics, Image Process. **45,** 295–345 (1989).
7. K.-S. Huang, B. K. Jenkins, and A. A. Sawchuk, "Image Algebra Representation of Parallel Optical Binary Arithmetic," Appl. Opt. **28,** 1263–1278 (1989).
8. C. C. Guest and T. K. Gaylord, "Truth-Table Look-Up Optical Processing Utilizing Binary and Residue Arithmetic," Appl. Opt. **19,** 1201–1207 (1980).
9. M. M. Mirsalehi and T. K. Gaylord, "Truth-Table Look-Up Parallel Data Processing Using an Optical Content-Addressable Memory," Appl. Opt. **25,** 2277–2283 (1986).
10. K.-H. Brenner, A. Huang, and N. Streibl, "Digital Optical Computing with Symbolic Substitution," Appl. Opt. **25,** 3054–3060 (1986).
11. K.-H. Brenner, "New Implementation of Symbolic Substitution Logic," Appl. Opt. **25,** 3061–3064 (1986).
12. A. Avizienis, "Signed-Digit Number Representations for Fast Parallel Arithmetic," IRE Trans. Electron. Comput. **EC-10,** 389–400 (1961).
13. R. P. Bocker, B. L. Drake, M. E. Lasher, and T. B. Henderson, "Modified Signed-Digit Addition and Subtraction Using Optical Symbolic Substitution," Appl. Opt. **25,** 2456–2457 (1986).
14. Y. Li and G. Eichmann, "Conditional Symbolic Modified Signed-Digit Arithmetic Using Optical Content-Addressable Memory Logic Elements," Appl. Opt. **26,** 2328–2333 (1987).

15. A. K. Cherri and M. A. Karim, "Modified-Signed Digit Arithmetic Using an Efficient Symbolic Substitution," Appl. Opt. **27**, 3824–3827 (1988).
16. B. Parhami, "Carry-Free Addition of Recoded Binary Signed-Digit Numbers," IEEE Trans. Comput. **C-37**, 1470–1476 (1988).
17. G. A. De Biase and A. Massini, "Redundant Binary Number Representation for Parallel Arithmetic on Optical and Electronic Computers," IEEE Trans. Comput. (1989), submitted.
18. N. Takagi, H. Yasuura, and S. Yajima, "High-Speed VLSI Multiplication Algorithm with a Redundant Binary Addition Tree," IEEE Trans. Comput. **C-34**, 789–796 (1985).
19. G. A. De Biase, "Trends in Astronomical Image Processing," Comput. Vision Graphics Image Process. **43**, 347–360 (1988).
20. G. A. De Biase, "Interconnection Structures and Parallel Computing," in *Advances in Parallel Computing*, D. J. Evans, Ed. (JAI Press, London, 1990), in press.

Multiple Fourier transform generation for coherent optical correlators

Juris Upatnieks, James O. Abshier, Charles R. Christensen, and John Stensby

Charles Christensen is with MICOM, AMSMI-RD-RE, Redstone Arsenal, Alabama 35890; John Stensby is with University of Alabama in Huntsville, Department of Electrical & Computer Engineering, Huntsville, Alabama 35899; the other authors are with Environmental Research Institute of Michigan, Optical Science Laboratory, Ann Arbor, Michigan 48107-8618.
Received 3 April 1989.
0003-6935/90/111589-02$02.00/0.

An interferometrically generated off-axis holographic optical element images a laser diode light source to a 3 × 5 point array through 10 cm of glass. The element also reduces the elliptical beam cross section from 3:1 to 1.5:1.

Practical utilization of coherent optical correlators requires compact designs which may include provisions for addressing multiple parallel filters. Compact correlator designs have been proposed in the past.[1,2] We describe here a compact correlator design featuring multiple Fourier transform filter addressing. A holographic optical element (HOE) was utilized to generate multiple Fourier transforms as well as to perform a number of other functions.

Figure 1 shows the layout of the optical system with three of the fifteen Fourier transforms (FTs) indicated. The input image is introduced by means of a liquid crystal light modulator.[3] A laser diode, rather than a helium–neon laser, is used as a light source for greater compactness. In this arrangement the HOE performs numerous functions: it reduces the elliptical cross section of the illuminating beam from a ratio of 3:1 to 1.5:1, it corrects for the astigmatism that would be expected from a diverging beam passing at a 60° angle of incidence through the HOE cover plate, it replaces both the collimating and the Fourier transform lenses that are used in the classical VanderLugt matched filter correlator,[4] and it corrects for the aberrations of multiple converging beams passing through the 10-cm thick polarizing beam splitter glass.

To achieve aberration-free performance the HOE was fabricated with the optical system shown in Fig. 2. The fifteen point sources were generated by an array of fifteen 5-mm diam HOEs recorded with a collimated reference beam. The recording plate was translated between exposures with precision translating stages. This insured exact spacing and the same focal lengths for all lenslets. The multiple FT HOE in Fig. 2 was recorded with a converging reference beam that included a tilted glass plate to correct for astigmatism and an array of fifteen point sources with a 10-cm long glass block between the sources and the HOE. The tilted plate was adjusted until aberrations in the reference beam disappeared as observed at the focus. Exact aberration correction for the multiple FT HOE requires the recording wavelength to be the same as the use wavelength, thus the HOE was also recorded with a laser diode. The recording was made with a 780-nm temperature-stabilized laser diode, adjusted for 20-mW output, in Kodak 120 emulsion. Due to low efficiency of the fifteen HOEs and the fast divergence of beams, light level was rather low at the HOE recording plane. To reduce the exposure time to a few minutes, a 20:1 reference-to-signal beam ratio was used and the plates were hypersensitized by soaking them in 1.12% solution of ammonium hydroxide and then drying them shortly before exposure. At 780 nm the hypersensitized plates had about 1/30 the sensitivity of the 120 emulsion at 633 nm, while plates without hypersensitization had a sensitivity of about 1/250 of that at 633 nm. The emulsion was processed to obtain a silver halide sensitized dichromated gelatin hologram.[5,6]

The multiple filter correlator was tested with a high contrast 18-cycle (alternating light–dark spoke) star target as the input image and a 30-mW 780-nm temperature-stabilized laser diode as the light source. The same filter was recorded at each filter position and the reference beam was arranged to give correlations in a pattern similar to the filter positions. The filters were recorded on Kodak 120 emulsion, developed in the usual way, and then partly bleached. A solution of iodine diluted with methanol, one part iodine to 50 parts of methanol, was prepared and then a few drops at a time were added to water in which the developed plate was

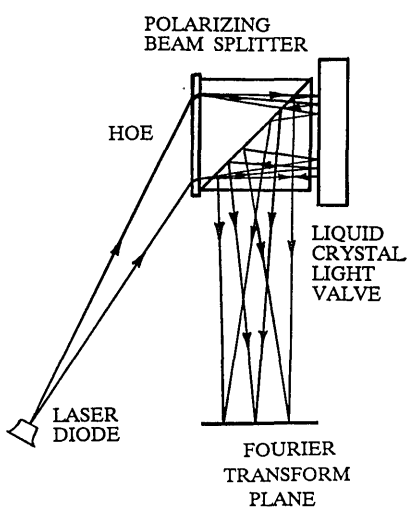

Fig. 1. Compact multiple Fourier transform optical system.

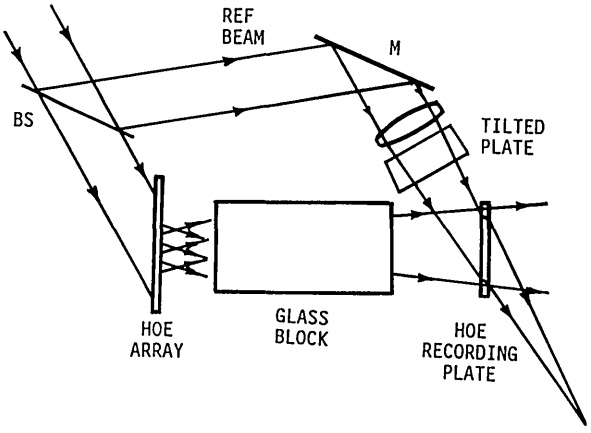

Fig. 2. Multiple Fourier transform HOE recording.

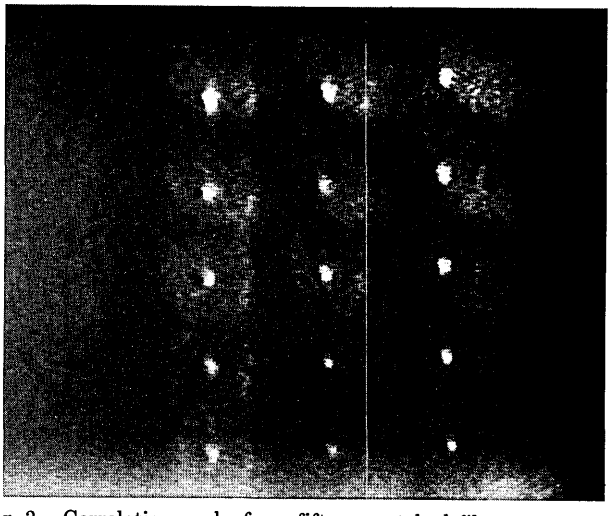

Fig. 3. Correlation peaks from fifteen matched filters correlated against one input image.

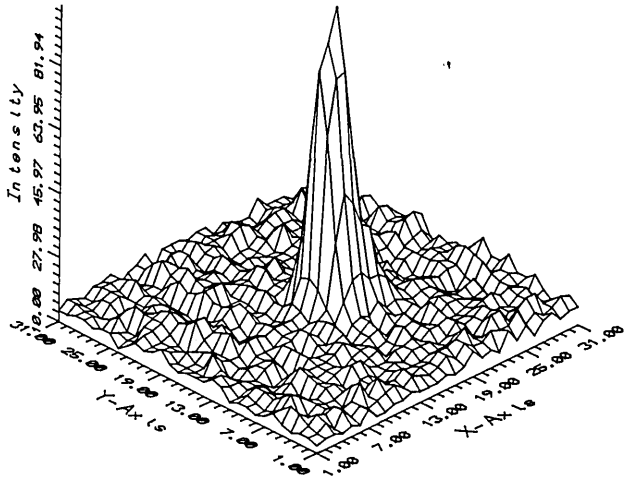

Fig. 4. Plot of one correlation peak.

submerged.[7] Bleaching was continued until the lightly exposed areas were completely bleached while the central spot of the filter remained opaque. With an opaque central spot the filter acts as a high pass filter, an important and desirable property in matched filter correlators.

Correlation peaks of the input target with the fifteen filters are shown in Fig. 3. While some variation in peak brightness is evident, this is related to the alignment accuracy of fifteen filters with fifteen Fourier transforms. Energy in each of the Fourier transforms was measured and found to be the same to within a few percent. Figure 4 shows a 2-D plot of one of the correlation peaks.

The method for generating multiple Fourier transforms described here helps in the reduction of the correlator system size and its weight. However, we observed that the signal beam has a highly nonuniform amplitude which limits the HOE efficiency. This is likely caused by the coherent addition of the fifteen wavefronts in the HOE recording plane. An analysis of this problem and improvement in the signal beam uniformity are needed. With improved uniformity, efficiencies in excess of 50% should be achieved.

References

1. J. G. Duthie, J. Upatnieks, C. R. Christensen, and R. D. McKenzie, Jr., "Real-Time Optical Correlation with Solid-State Sources," Proc. Soc. Photo-Opt. Instrum. Eng. **231**, 281–290 (1980).
2. J. G. Duthie and J. Upatnieks, "Compact Real Time Coherent Optical Correlators," Opt. Eng. **23**, 7–11 (1984).
3. W. P. Bleha *et al.*, "Application of the Liquid Crystal Light Valve to Real Time Optical Processing," Opt. Eng. **17**, 371–384 (1978).
4. A. VanderLugt, "Signal Detection by Complex Spatial Filtering," IEEE Trans. Inf. Theory **IT-10**, 139–145 (1964).
5. W. P. Graver, J. W. Gladden, and J. W. Eastes, "Phase Holograms Formed by Silver Halide (Sensitized) Gelatin Processing," Appl. Opt. **19**, 1529–1536 (1980).
6. B. J. Chang and K. Winick, "Silver-Halide Gelatin Holograms," Proc. Soc. Photo-Opt. Instrum. Eng. **215**, 172–177 (1980).
7. A procedure developed by C. D. Leonard, Environmental Research Institute of Michigan; private communication.

Generalization of the backpropagation neural network learning algorithm to permit complex weights

Gordon R. Little, Steven C. Gustafson, and Robert A. Senn

When this work was done all authors were with University of Dayton, Research Institute, Dayton, Ohio 45469-0007; R. A. Senn is now with Eastman Kodak Company, Rochester, New York 14650.

Received 4 April 1989.
0003-6935/90/111591-02$02.00/0.

The backpropagation neural network learning algorithm is generalized to include complex-valued interconnections for possible optical implementations.

Neural networks and neural network simulations are generally formed from large numbers of well-interconnected but relatively simple analog elements. Since optical interconnections are naturally noninterfering and optical components are typically analog, it is widely recognized that neural networks could have efficient optical implementations. Many proposed optical implementations[1–3] use multiple coherent optical beams to represent signals, holographic gratings for interconnection (weighting), and nonlinear optical or optoelectronic arrays for processing. In such architectures, optical signals and weights are appropriately described using complex numbers, when both magnitude and phase information are included. However, with a few exceptions,[4–7] complex interconnection weights have not been considered in neural network models.

The backpropagation learning algorithm[8] is by far the most widely used procedure for training feed-forward neural networks that solve practical recognition and classification problems. Model optical implementations[3,9] of this algorithm have been proposed. A generalization of backpropagation to include complex weights and thresholds is described below. This generalization is directed toward optical implementations in which the nonlinear operation in a neuron is a function only of the optical intensity at the neuron. This mode of operation is clearly appropriate when the nonlinear operation is implemented optoelectronically using direct detection followed by electronic thresholding, and it may be applicable for many all-optical nonlinear processes. The transmission of a saturable absorber, for example, depends on the amount of energy absorbed.

Our neural network model as depicted in Fig. 1 has I external inputs, J neurons in a hidden layer, and K neurons in the output layer. We use subscript i to index inputs, and subscripts j and k to index neurons in the hidden and output layers, respectively. The ith external input is y_i while the outputs of the jth (kth) neurons in the hidden (output) layer are y_j (y_k). Superscripts r and i are used to index the real and imaginary parts of a parameter, and a nonsubscripted i is $\sqrt{-1}$. In this notation, $w_{ij}^r + iw_{ij}^i$ represents the complex interconnection weight between input i and hidden layer neuron j while $w_{jk}^r + iw_{jk}^i$ represents the complex weight between hidden layer neuron j and output layer neuron k. Following Ref. 8, we use the symbol net j (net k) to represent the total complex input to the jth (kth) neuron in the hidden (output) layer, i.e.,

$$\text{net}_k^{r/i} = \sum_j w_{jk}^{r/i} y_j + w_{ok}^{r/i}, \tag{1a}$$

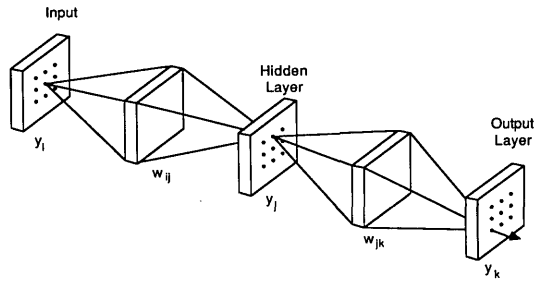

Fig. 1. Visualization of an optically implemented, feed-forward neural network. External inputs are represented by an array of mutually coherent point sources, neurons in the hidden and output layers are represented by arrays of nonlinear processing elements, and interconnections are provided by multiplexed holograms.

$$\text{net}_j^{r/i} = \sum_i w_{ij}^{r/i} y_i + w_{oj}^{r/i}. \tag{1b}$$

Here r/i indicates that either the r or i superscript is to be used consistently in the expression; the sums over i and j are from 1 to I and 1 to J, respectively; the the $w_{ok}^{r/i}$ and $w_{oi}^{r/i}$ weights represent thresholds (or offsets). With these conventions, the neuron outputs are

$$y_k = g[(\text{net}_k^r)^2 + (\text{net}_k^i)^2], \tag{2a}$$

$$y_j = g[(\text{net}_j^r)^2 + (\text{net}_j^i)^2]. \tag{2b}$$

Note that the nonlinearity here is described as a two-stage process, the explicit coherent-to-incoherent conversion operation and the as-yet-unspecified function g. Clearly one form of g which is of interest is the sigmoid nonlinearity $g(x) = [1 + \exp(-x)]^{-1}$ commonly used in standard backpropagation. However, the first stage nonlinearity allows useful network computation even if a linear function $[g(x) = x]$ is used in Eqs. (2a) and (2b).

Suppose that when the neural network inputs are y_i the desired outputs are d_k. Then the weights $w_{jk}^{r/i}$, $w_{ok}^{r/i}$, $w_{ij}^{r/i}$, $w_{oj}^{r/i}$, are to be found such that a quantity E proportional to the sum of squared errors is minimized, where

$$E = \frac{1}{2} \sum_k (d_k - y_y)^2. \tag{3}$$

In general the above weights will have nonzero values due to prior training or due to the selection of small random initial values. Thus the problem reduces to finding optimum weight changes. For weights terminating on output neurons,

$$\Delta w_{jk}^{r/i} = -\eta \frac{\partial E}{\partial w_{jk}^{r/i}} = \eta \delta_k^{r/i} y_j, \tag{4}$$

where η is a gain parameter and

$$\delta_k^{r/i} = -\frac{\partial E}{\partial \text{net}_k^{r/i}} = 2(d_k - y_k)\text{net}_k^{r/i} g_k'. \tag{5}$$

Here g_k' represents the derivative of the nonlinearity function as evaluated for the kth neuron. For weights terminating on hidden neurons,

$$\Delta w_{ij}^{r/i} = -\eta \frac{\partial E}{\partial w_{ij}^{r/i}} = \eta \delta_j^{r/i} y_i, \tag{6}$$

where

$$\delta_j^{r/i} = -\frac{\partial E}{\partial \mathrm{net}_j^{r/i}}$$

$$= \sum_k \delta_k^r w_{jk}^r 2\mathrm{net}_j^{r/i} g_j' + \delta_k^i w_{jk}^i 2\mathrm{net}_j^{r/i} g_j'. \tag{7}$$

Results collected from Eqs. (4), (5), (6), and (7) are

$$\Delta w_{jk}^{r/i} = \eta \delta_k^{r/i} y_j, \tag{8a}$$

$$\delta_k^{r/i} = 2\mathrm{net}_k^{r/i}(d_k - y_k) g_k', \tag{8b}$$

$$\Delta w_{ij}^{r/i} = \eta \delta_j^{r/i} y_i, \tag{9a}$$

$$\delta_j^{r/i} = 2\mathrm{net}_j^{r/i} \sum_k (\delta_k^r w_{jk}^r + \delta_k^i w_{ik}^i) g_j'. \tag{9b}$$

A notable feature of these results is that both δ_j^r and δ_j^i depend separately on both δ_k^r and δ_k^i. Note also that Eqs. (8b) and (9b) require that the total input to each neuron be available during computation of the delta values. This is deemed a relatively minor cost in that it requires additional storage equal to the number of neurons ($I + J$) rather than the number of interconnections ($IJ + JK$).

Tests of the complex weight backpropagation algorithm were made using computer simulations. These simulations used a linear function for g and investigated the EXCLUSIVE-OR logic problem. A neural network consisting of two inputs, two hidden-layer neurons, and one output neuron was used. The weight adaptation Eqs. (8a) and (9a) were modified to include the momentum term commonly used in backpropagation[8]:

$$\Delta w_{jk}^{r/i} = \eta \delta_k^{r/i} y_j + \alpha \Delta w_{jk}^{r/i}, \tag{10}$$

$$\Delta w_{ij}^{r/i} = \eta \delta_j^{r/i} y_i + \alpha \Delta w_{ij}^{r/i}. \tag{11}$$

We found that small gain values ($\eta \leq 0.05$) were necessary to prevent learning from becoming unstable. Optimum performance, as measured by learning speed, was achieved for $\eta = 0.01$ and $\alpha = 0.9$. The learning curve for this case is shown in Fig. 2 along with the learning curve obtained using the standard backpropagation algorithm with gain and momentum of $\eta = 0.3$ and $\alpha = 0.9$. An order of magnitude improvement in learning speed is noted for the complex weight case. However, such a dramatic improvement may not persist for other choices of algorithm parameters or for larger or more complex problems.

Recently, a somewhat different generalization of backpropagation to complex-valued weights was described.[7] This approach is an extension of the complex Widrow-Hoff least mean-square adaptive algorithm[6] in which neuron outputs as well as weights are allowed to be complex. In addition, the nonlinear function g is applied separately to both the real and imaginary parts of the total input to the neurons. This scheme is not as appropriate for optical implementation as is our scheme.

As noted earlier, neural network modeling has traditionally used only real-valued weights, presumably because this choice is more nearly correct from a biological point of view. We adopt the pragmatic view that, if the aim is to solve engineering problems, biological plausibility need not be retained. It is interesting to note, however, that Noest,[5] who examined the use of complex weights in Hopfield nets, suggests that phase information may be important in describing biological interconnections.

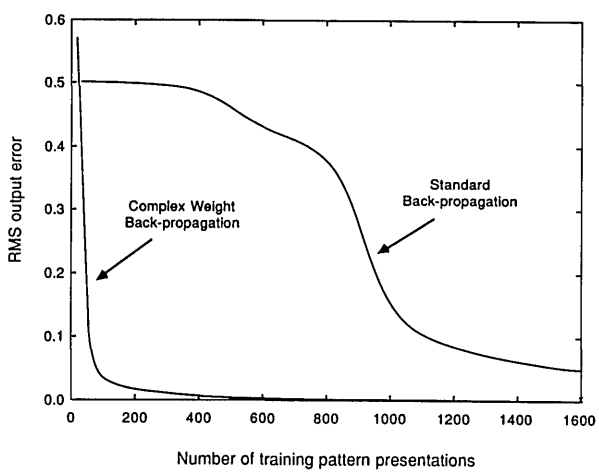

Fig. 2. Simulation results for the EXCLUSIVE-OR logic function implemented with two hidden neurons and a single output neuron. Gain (η) and momentum (α) parameters used are $\eta = 0.01$ and $\alpha = 0.9$ for the complex weight backpropagation simulation and $\eta = 0.3$ and $\alpha = 0.9$ for the standard backpropagation simulation.

References

1. S. C. Gustafson and G. R. Little, "Neural Network Models Based on Optical Resonator Designs," in *Technical Digest, Topical Meeting on Optical Computing* (Optical Society of America, Washington, DC, 1989), paper TUI20.
2. K. Wagner and D. Psaltis, "Multilayer Optical Learning Networks," Appl. Opt. **26**, 5061–5076 (1987).
3. Y. Owechko, "Optoelectronic Resonator Neural Networks," Appl. Opt. **26**, 5104–5111 (1987).
4. S. C. Gustafson, "Thresholding and Weighting in Optical Computing," *Optical Computing*, R. Arrathoon, Ed. (Marcel Dekker, New York, 1989).
5. A. J. Noest, "Phasor Neural Networks," in *Neural Information Processing Systems*, D. Z. Anderson, Ed. (American Institute of Physics, New York, 1988).
6. B. Widrow, J. McCool, and M. Ball, "The Complex LMS Algorithm," Proc. IEEE **63**, 719–720 (1975).
7. D. L. Birx and S. J. Pipenberg, "Neural Network Structures for Defect Discrimination," presented at Fifth Annual Aerospace Applications of Artificial Intelligence Conference, Dayton, OH 24–26 Oct. 1989.
8. D. E. Rumelhart, G. E. Hinton, and R. J. Williams, "Learning Internal Representations by Error Propagation," *Parallel Distributed Processing*, D. E. Rumelhart and J. L. McClelland, Eds. (MIT Press, Cambridge, MA, 1986).
9. D. Psaltis, D. Brady, and K. Wagner, "Adaptive Optical Networks Using Photorefractive Crystals," Appl. Opt. **27**, 1752–1759 (1988).

Attenuation measurement in liquids by analysis of the space–time structure of backscattered laser light pulses

Jean Lotrian, Jack Cariou, and Yves Guern

Universite de Bretagne Occidentale, Faculte des Sciences, Laboratoire de Spectrometrique et Optique Laser, F-29287 Brest CEDEX, France.

Received 29 July 1988.
0003-6935/90/111593-02$02.00/0.

We underline the experimental feasibility of the extinction coefficient measurement $c = a + b$ (a is the absorption coefficient, b is the diffusion coefficient) for a liquid medium, extracted from the temporal shape of the backscattered signal at 180° to the incident laser pulses.

This method using a pulsed laser was initially tried out on pure water, loaded with scattering particles corresponding to c extinction coefficients from 0.1 to 1.5 m^{-1}. The possibility of extracting certain optical characteristics of liquid media from backscattered light has only been published for a few experimental or theoretical works.[1–4] The work described here concerns the propagation of a laser beam at close range (only a few meters).

A single scattering treatment of the backscattered light pulses shows that time spreading can be expressed by

$$R(t) = P(t) * T(t), \tag{1}$$

where $P(t)$ concerns the incident light pulse, and

$$T(t) = \frac{v}{2n}\beta(180)\exp-\frac{cvt}{n}\cdot\Omega(t) \tag{2}$$

is the impulse response of the medium with $\Omega(t) = 1/(nl + vt/2n)^2$, c is the extinction coefficient, $\beta(180)$ is the backscattered diffusion coefficient, v/n is the celerity of the electromagnetic wave, n is the refractive index, and l is the distance from the detector to the scattering medium.[5]

For a very short laser pulse (Dirac pulse) Eq. (1) simplifies to

$$R(t) = [K\exp(-cvt/n)]/(2nl + vt/n)^2,$$

and the c value is obtained from the shape of the

$$\log[R(t)(2nl + vt/n)^2] = K' - cvt/n,$$

which may become more complicated due to the eventual presence of a multiple scattered component. However simulations using a semianalytical Monte Carlo treatment as described by Poole *et al.*[6] have shown that this contribution is limited in experimental conditions (according to the small numerical aperture of the detection system and a maximum c value of 1.5 m^{-1}).

Figure 1 shows the experimental setup; the temporal shape of the signal backscattered in the propagation medium is obtained in the R_1 direction. The measurement of the global extinction coefficient is obtained from differential measurements of the 90° scattering along the laser beam direction (with a single detector successively placed at 0.6 and 3 m from the entrance window of the experimental tank).

The light source used was a pulsed dye laser pumped by a nitrogen laser (4-ns pulse duration) and tuned to 532 nm. The incident light was linearly polarized; the detection was

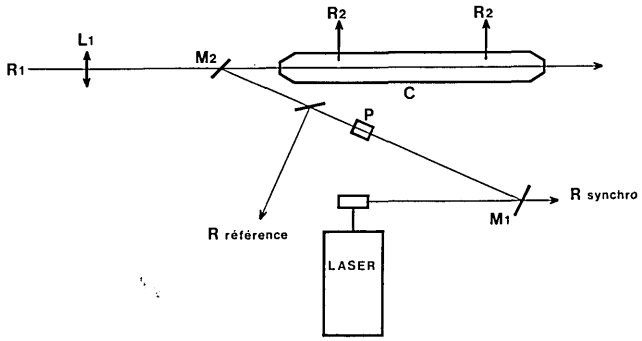

Fig. 1. Experimental setup: dye laser with 4-ns pulse duration; R_1, detector for the backscattered signal; R_2, lateral detector; M_2, 5- × 10-mm mirror.

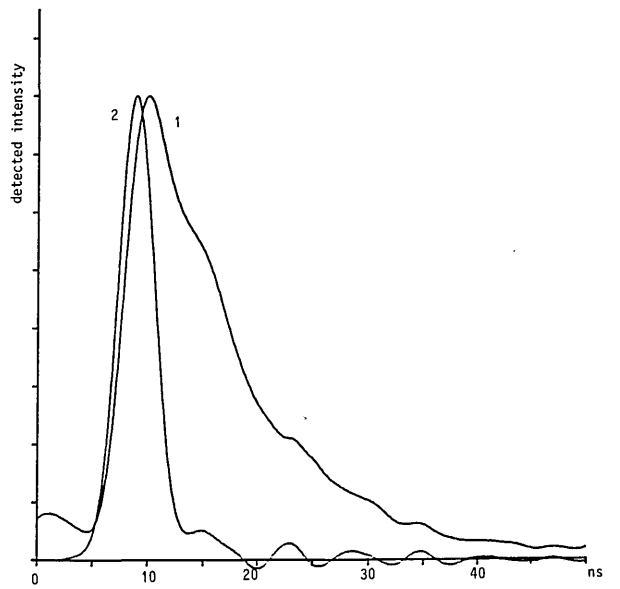

Fig. 2. Backscattered signal in distilled water with c = 0.08 m^{-1} (trace 1) and backscattered signal from a diffuse target (trace 2) at the entrance of curve c (temporal reference). The first maxima in trace 1 can be attributed to diffusion on the M_2 small mirror.

global and analyzed by a transient digital analyzer (Tektronix 7912).

Figure 2 shows an experimental shape obtained in pure water (c = 0.08 m^{-1}) and the laser pulse probe detected [corresponding to $P(t)$ in Eq. (1)].

Figure 3 shows experimental profiles obtained using pure water with added calibrated clay powder (with 85% of the diameter of the particles between 1.6 and 3.5 μm) for c values corresponding to 0.1 and 0.45 m^{-1}.

A comparison is made in Table I between the two methods of c measurement from the shape of the backscattered light and from lateral differential scattering. Good agreement was found using various samples of water with different quantities of clay powder added. According to the respective accuracy of the different measurements on each sample, the standard deviation was found between 10^{-2} and 5×10^{-2} m^{-1}. All these tests were undertaken using a total of 640 individual light pulses.

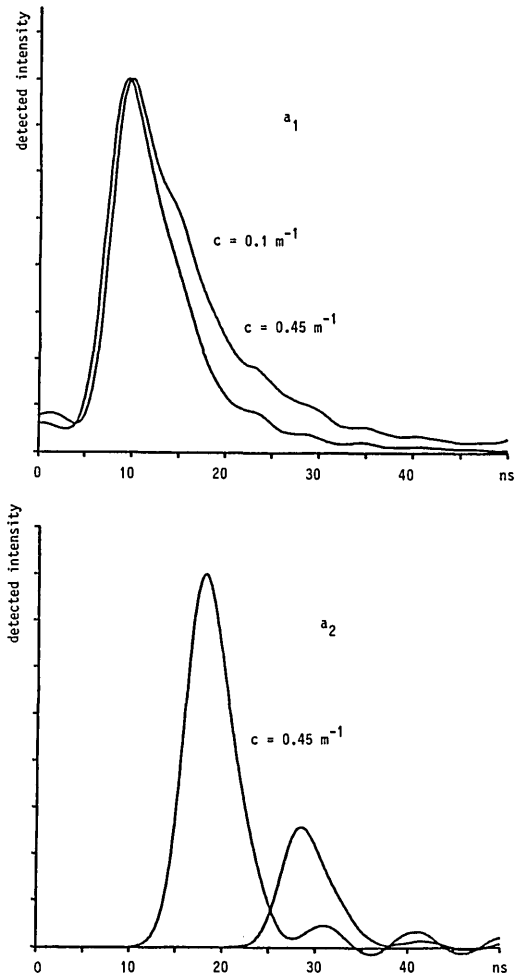

Fig. 3. Experimental normalized traces from a backscattered signal (a_1) and a 90° diffuse signal (a_2) using distilled water with kaolinite powder added for $c = 0.45$ m^{-1}.

Table I. c Values in m^{-1} (Pure Water + Clay Powder)

Backscattered method	Lateral scattering
0.08	0.085 pure water
0.19	0.21 pure water + 0.3 mg/l
0.45	0.44 + 0.9 mg/l
0.80	0.85 +2.25 mg/l
1.13	1.13 +3.80 mg/l

The advantages of using a backscatter measuring technique are twofold: first, the laser and detector can be used independent of the medium studied and second, the technique can be used to pinpoint optical inhomogeneity.

This work was supported by the Direction des Recherches Etudes et Techniques under grant 84.155.

References

1. E. P. Zege, A. P. Ivanov, B. A. Kargai, and I. L. Katrev, "Determination of the Attenuation and Scattering Coefficients of Water and the Atmosphere from the Time Spread of a Reflected Pulsed Signal," Bull. Acad. Sci. URSS Atmos. Oceanic Phys. 8, 10–16 (1972).
2. L. R. Poole, "Computed Laser Backscattering from Turbid Liquids: Comparison with Laboratory Results," Appl. Opt. 21, 2262–2264 (1982).
3. D. Bright and J. W. Caruthers, "The Effect of Detector Field-of-View on Laser Backscatter and Bottom Reflection Measurements," Proc. Soc. Photo-Opt. Instrum. Eng. 489, 281–286 (1984).
4. H. S. Lee and N. T. O'Neill, "Lidar Return Pulse Profile and Its Relationship to Water Optical Parameters," Proc. Soc. Photo-Opt. Instrum. Eng. 489, 297–305 (1984).
5. H. R. Gordon, "Interpretation of Airborne Oceanic Lidar: Effects of Multiple Scattering," Appl. Opt. 21, 2996–3001 (1982).
6. L. R. Poole, D. D. Venable, and J. W. Campbell, "Semianalytic Monte Carlo Radiative Transfer Model For Oceanographic Lidar Systems," Appl. Opt. 20, 3653–3656 (1981).